

MOFs-Templated Co@Pd Core–Shell NPs Embedded in N-Doped Carbon Matrix with Superior Hydrogenation Activities

Kui Shen,[†] Liang Chen,[‡] Jilan Long,[†] Wei Zhong,[†] and Yingwei Li^{*,†}

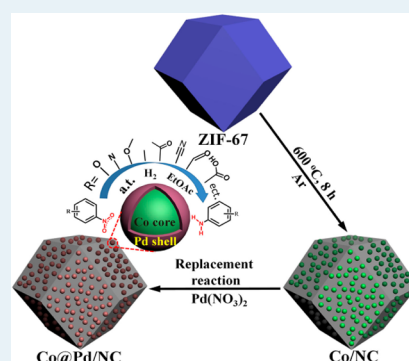
[†]School of Chemistry and Chemical Engineering, South China University of Technology, Guangzhou 510640, People's Republic of China

[‡]Department of Chemistry and Collaborative Innovation Center of Chemistry for Energy Materials, Fudan University, 220 Handan Road, Shanghai 200433, People's Republic of China

S Supporting Information

ABSTRACT: Although MOFs supporting noble metal nanoparticles (NPs) have been widely used in heterogeneous catalysis, they are still limited in catalytic efficiency on a per-noble-metal-atom basis. Here we developed a MOFs-templated strategy to non-noble metal @noble metal core–shell nanocatalysts, which could far surpass the traditional MOFs supporting noble NPs in catalytic properties, by using MOFs-derived metal NPs as sacrificial templates to reduce noble metal ions via galvanic replacement reaction. As a model system, Co@Pd core–shell NPs embedded in the N-doped carbon matrix (Co@Pd/NC) were synthesized with an average size of ca. 9.4 nm and a ultrathin Pd shell by using ZIF-67 and Pd(NO₃)₂ as the precursor and Pd source, respectively. The highly exposed Pd atom on Co nanoparticles made it an attractive catalyst with high efficiency. When being used in the hydrogenation of nitrobenzene, the Co@Pd/NC exhibited an unprecedented high activity over Pd-based catalysts, yielding 98% conversion after 45 min reaction, which was far more active than the pristine ZIF-67 and MIL-101 supporting Pd NPs (with 40% and 3% conversion after 90 min reaction, respectively) under identical conditions, suggesting its overwhelmingly better performance than MOFs supporting noble NPs. We anticipated that this strategy would form the basis for developing a new class of MOF-templated core–shell nanocatalyst with potential applications in numerous catalytic reactions.

KEYWORDS: core–shell structure, heterogeneous catalysis, metal–organic frameworks, nanoparticles, noble metal



INTRODUCTION

Metal–organic frameworks (MOFs) built from metal ions and polyfunctional organic ligands are attractive and significant materials for many industrial applications due to their excellent chemical and physical properties such as extra high specific surface area, well-defined pore structure, and low density.¹ Particularly, MOFs provide a tunable coordination space and chemical tailoring of the inner surface of the channels and cavities, which make them a promising new class of catalyst supports for hosting nanoparticles, especially for noble metal nanoparticles (MNPs) in heterogeneous catalysis.² Over the past decades, research efforts have been mostly aimed at preparing new MOFs structures and developing new approaches for loading MNPs more effectively inside the porous matrices of MOFs.² A few examples are Pd, Au, Pt, Ru, Ir, Au–Pd, Ni–Pd nanoparticles stabilized on different MOF structures by employing various techniques such as chemical vapor deposition (CVD),³ impregnation,⁴ solid grinding,⁵ colloidal deposition method,⁶ and double solvents approach.⁷ However, in spite of these promising approaches, the MOFs supporting noble NPs are still limited in catalytic performance because of the following two reasons: (1) Most of the MOFs are known to have intrinsically weaker material properties such as low thermal stability,⁸ extreme sensitivity to air,⁹ water,¹⁰

acids,¹¹ and bases,¹¹ and poor electrical conductivity,¹² which hinder their applications for catalysis; (2) The noble NPs supported on MOFs by the existing methods are mostly several nanometers in diameter,^{3–7} resulting in the lack of sufficient active centers and the optimal microstructure. Apparently, alternative concepts and strategies have to be devised to break the above two bottlenecks and develop novel supported noble metal catalysts with high efficiencies.

More recently, MOFs were proved to be ideal sacrificial templates for fabricating porous carbon-based nanomaterials via thermal decomposition under controlled atmospheres.^{8b,13} In particular, by calcining the MOFs containing the metal centers with a reduction potential of 0.27 V or higher in inert atmosphere, these metal ions of MOFs could be transformed into metal NPs, which are embedded in a ligand-derived porous carbon matrix.¹⁴ Inspired by these advances, herein, we propose a facile and efficient approach to fabricate non-noble metal@noble metal core–shell nanocatalysts by using MOFs-derived metal NPs as sacrificial templates to reduce noble metal ions via galvanic replacement reaction. Co@Pd core–shell nano-

Received: May 13, 2015

Revised: July 6, 2015

Published: July 30, 2015

particles embedded in N-doped carbon matrix (denoted as Co@Pd/CN) were successfully prepared as a model to verify this strategy by using ZIF-67 and Pd(NO₃)₂ as the precursor and Pd source, respectively. The highly exposed Pd atom on Co nanoparticles made it excellent as a highly active, extremely stable nanocatalyst toward the nitrobenzene hydrogenation reaction. The Co@Pd/NC showed 98% conversion of nitrobenzene after a 45 min reaction, which was far more active than the pristine ZIF-67 and MIL-101 supporting Pd NPs (with 40% and 3% conversion after 90 min reaction, respectively) under identical conditions.

EXPERIMENTAL SECTION

Chemicals. Methylimidazole (MeIM, 98%), cobalt nitrate (Co(NO₃)₂·6H₂O, > 99%), benzenedicarboxylate (H₂bdc, > 99%) and chromium(III) nitrate nonahydrate were purchased from Aladdin Industrial Corporation. Palladium nitrate dihydrate was purchased from Shanghai yuanye Bio-Technology Co., Ltd. The activated charcoal was purchased from Sigma-Aldrich.

Synthesis of ZIF-67. The preparation of ZIF-67 polyhedrons (Co(MeIM)₂, MeIM = 2-methylimidazole) was based on a reported method¹⁵ with some modifications. In a typical synthesis, 0.45 g of cobalt nitrate hexahydrate was dissolved in 3 mL of deionized water. Then another solution was prepared by dissolving 5.5 g of 2-methylimidazole in 20 mL of deionized water. The former solution was poured into the later one under magnetic stirring, resulting in a mixture with molar composition of 1 Co²⁺/58 MeIM/1100 H₂O. After keeping stirring for 6 h at room temperature, the resulting purple precipitates were washed thoroughly with water, and finally dried under vacuum at 80 °C for 24 h.

Synthesis of Co/NC Materials by Thermolysis of ZIF-67. The typical procedure for the preparation of the Co/NC materials was described as follow: 2 g of ZIF-67 was pyrolyzed at 600 °C with a heating rate of 1 °C/min from room temperature under continuous Ar flow. After reaching the target temperature, the material was held at this temperature for 8 h and then cooled to room temperature.

Synthesis of Co@Pd/NC Based on Galvanic Replacement Reaction. In a standard procedure, 0.4 g of as-prepared Co/NC was initially dispersed in 20 mL of acetone to form a uniform suspension via ultrasonication for 5 min. Then, 5 mL of acetone solution containing a required amount of Pd(NO₃)₂ was added dropwise under magnetic stirring at room temperature. The resultant mixture was reacted for another 12 h. All the synthetic processes were conducted under an Ar atmosphere as the Co NPs were easily oxidized in air. The Co@Pd/NC formed was recovered by an external magnetic field, washed several times with acetone, and dried under vacuum at 50 °C.

Synthesis of MIL-101. MIL-101 was synthesized by the hydrothermal method according to a previous literature.¹⁶ Cr(NO₃)₃·9H₂O (99%) (2.007 g, 5.0 mmol), HF (48 wt %, 5.0 mmol), terephthalic acid (98%, 0.823 g, 5.0 mmol), and 24 mL of deionized water were mixed completely and heated at 220 °C for 8 h. Subsequently, the mixture was cooled slowly to room temperature. The resulting green powder of MIL-101 with formula Cr₃F(H₂O)₂O[(O₂C)C₆H₄(CO₂)]₃·nH₂O (*n* ≤ 25) was doubly filtered off using two glass filters with pore sizes between 40 and 100 μm to remove the unreacted crystals of terephthalic acid, and further soaked in ethanol (95% EtOH with 5% water) at 80 °C for 24 h. Finally, the resulting MIL-

101 was dried overnight at 150 °C under vacuum for further use.

Synthesis of Pd/MIL-101, Pd/ZIF-67, Pd/C, Pd/NC, and Pd-Co/MIL-101. All of Pd/MIL-101, Pd/ZIF-67, and Pd/C were prepared via a conventional impregnation method by using MIL-101, ZIF-67 and activated charcoal as the supports. Typically, 0.6 g of support (MIL-101/ZIF-67/activated charcoal) was dispersed in 20 mL of acetone and was stirred for 20 min at room temperature. Five milliliters of Pd²⁺ acetone solution containing 0.03 g of Pd(NO₃)₂·2H₂O was added dropwise to the above solution under magnetic stirring for about 10 min. The flask containing the slurry was subjected to ultrasonication for 20 min and was then magnetically agitated at room temperature for 24 h. The impregnated samples were washed with acetone until the filtrate became colorless and then was slowly dried under air at room temperature for 24 h. The as-synthesized samples were further dried at 150 °C for 8 h, followed by treating in a stream of H₂ at 200 °C for 2 h to obtain Pd/MIL-101, Pd/ZIF-67, and Pd/C. In order to study the role of N in the activity of Co@Pd/NC, we also prepared Pd/NC by the above impregnation method with NC as the support, which was obtained by etching away Co NPs in Co/NC using aqua regia. Based on atomic absorption spectroscopy (AAS) analysis, the Pd loadings in the Pd/MIL-101, Pd/ZIF-67, Pd/C, and Pd/NC were 1.02, 0.87, 1.21, and 0.71 wt %, respectively. Besides, Pd-Co/MIL-101 was also prepared by a colloidal deposition method. Briefly, 0.059 g of PVP (MW = 24000) was added to an aqueous solution (20 mL) containing 0.005 g Pd(NO₃)₂·2H₂O and 0.0099 g Co(NO₃)₂·6H₂O. The mixture was stirred for 0.5 h at 0 °C. Then, a freshly prepared aqueous solution of NaBH₄ (0.02 g) was rapidly added to the above mixture under vigorous stirring. After sol formation in a few minutes, 0.2 g activated MIL-101 was immediately added, and the solution was further stirred for 10 h. After washing thoroughly with deionized water, the obtained solid was further dried at 80 °C for 5 h under vacuum to obtain the final Pd-Co/MIL-101 (the Pd and Co loadings in the Pd-Co/MIL-101 were 0.87, and 0.61 wt %, respectively).

Characterization. Powder X-ray diffraction patterns of the samples were obtained on a Rigaku diffractometer (D/MAX-III A, 3 kW) using Cu K α radiation (40 kV, 30 mA, λ = 0.1543 nm). BET surface area and pore size measurements were performed with N₂ adsorption/desorption isotherms at 77 K on a Micromeritics ASAP 2020 instrument. Before measurements, the samples were degassed at 100 °C for 12 h. TGA-DSC of ZIF-67 was performed on a NETZSCH STA449C under argon atmosphere. X-ray photoelectron spectroscopy (XPS) measurements were performed on a Kratos Axis Ultra DLD system with a base pressure of 10⁻⁹ Torr. The Co and Pd contents in the samples were measured quantitatively by atomic absorption spectroscopy (AAS) on a HITACHI Z-2300 instrument. Elemental analysis was performed on a Elementar Vario EL III equipment. The size and morphology of materials were studied by high-resolution scanning electron microscopy (HR-SEM, S-3700N of HITACHI) equipped with an energy dispersive X-ray spectroscopy (EDX), and high-resolution transmission electron microscopy (HR-TEM, C/M300 of Philips). The elemental mappings were performed on a scanning transmission electron microscope (STEM) unit with a high-angle annular-dark-field (HAADF) detector (HITACHI S-5500) operating at 200 kV. The samples for TEM test were prepared by dissolving the samples in ethanol and then ultrasound for 30 min. After that, a very small amount of

suspensions were taken out using microsyringe and then dropped on a copper online. Raman spectra of the carbonized samples were obtained at room temperature with a LabRAM Aramis Raman system with a laser of 532 nm.

Hydrogenation of Nitrobenzene. Typically, a calculated amount of Co@Pd/NC (0.2 mol %) in ethyl acetate (2 mL) was placed in a 25 mL Schlenk tube, and nitrobenzene (0.062 g, 0.5 mmol) was added to the mixture under H₂ (1 atm) with a magnetic stirrer to initiate the reaction. After completion of the reaction, the catalyst was removed from the solution by magnetic field, and the liquid phase was subsequently analyzed by GC/MS (Shimadzu GCMS-QP5050A equipped with a 0.25 mm × 30 m DB-WAX capillary column). In addition to nitrobenzene, an array of nitro-substrates was also subjected to the Co@Pd/NC using the same Pd/substrate molar ratio. The recyclability of the Co@Pd/NC catalyst was investigated for the hydrogenation of nitrobenzene under an appropriate reaction condition (0.67 mmol nitrobenzene in 2 mL of EtOAc, magnetically stirring, H₂ balloon, room temperature, catalysts: 0.15 mol % Pd, 45 min of reaction time) by using the recovered catalysts. Each time, the catalyst was isolated from the solution by magnetic field after reaction, washed several times with ethyl acetate, dried under vacuum to remove the residual solvent, and then reused as the catalyst in the next run.

RESULTS AND DISCUSSION

Figure 1 schematically illustrated the procedure used herein to prepare Co@Pd/CN. A well-studied zeolitic imidazolate

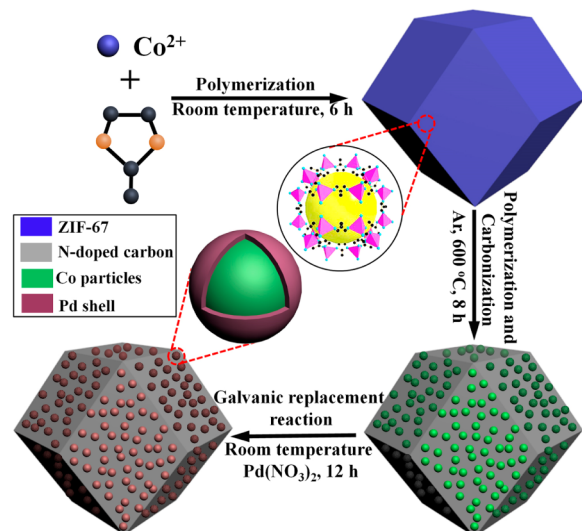


Figure 1. Schematic illustration of the process used for the synthesis of Co@Pd/NC.

framework material, ZIF-67, was first prepared from cobalt nitrate and 2-methylimidazole according to a facile room-temperature method.^{14,15} XRD patterns of as-synthesized ZIF-67 (Figure 2d and Figure S1) matched exactly with the simulated and also the published XRD patterns,^{16,17} confirming the product as phase-pure ZIF-67 with good crystallinity. SEM (Figure 2a and S5a) images clearly revealed the formation of polyhedral ZIF-67 with a smooth surface. Co NPs embedded in N-doped carbon were then synthesized by carbonizing ZIF-67 in an inert gas. During the pyrolysis process, the ligands of ZIF-67 (2-methylimidazole) were subjected to carbonization, while the Co²⁺ species were reduced to metallic Co.^{14a} The resulting

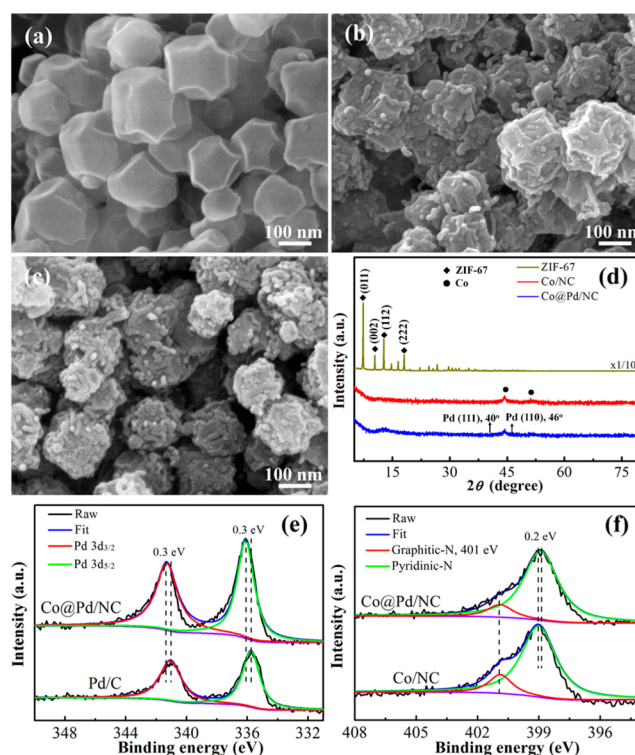


Figure 2. Typical SEM images of (a) ZIF 67, (b) Co/NC and (c) Co@Pd/NC. (d) XRD patterns of ZIF-67, Co/NC and Co@Pd/NC. (e) Pd 3d XPS spectra of Co@Pd/NC and Pd/C. (f) N 1s XPS spectra of Co@Pd/NC and Co/NC.

nitrogen–carbon composite played an important role in confining the Co species, leading to high dispersion of the Co NPs throughout carbon matrix with less aggregation. Because the standard reduction potential of the Co/Co²⁺ pair (−0.28 V vs the standard hydrogen electrode, SHE) was much lower than that of the Pd²⁺/Pd pair (0.8 V vs SHE), Pd²⁺ were reduced to Pd⁰ (by the galvanic displacement reaction: Co⁰ + Pd²⁺ → Co²⁺ + Pd⁰) and deposited on the surface of Co NPs, when Co/NC and Pd(NO₃)₂ were mixed in an aqueous medium, forming novel Co@Pd core–shell nanomaterial. The Co and Pd contents in the Co@Pd/NC materials were 30.7 and 1.1 wt %, respectively (Table S2). For comparison, Pd NPs supported ZIF-67, MIL-101 and activated charcoal (denoted as Pd/ZIF-67, Pd/MIL-101, and Pd/C, respectively) were also prepared by a conventional impregnation method.

The key idea of our method for synthesis of the Co@Pd/NC was to exploit the efficient growth of Pd shell on the core Co NPs through the replacement reaction. Obviously, smaller Co nanoparticles with higher active surface should be beneficial for the deposition of ultrathin Pd layer and thereby for enhanced catalytic activity. Thus, we initially studied the effect of pyrolysis temperature on the properties of resultant products. According to the TGA-DSC curves (Figure S2), the ZIF-67 precursor was highly stable up to 570 °C where they began to decompose. So, four different calcination temperatures (600, 700, 800, and 900 °C) were applied with a heating rate of 1 °C/min from room temperature. The TEM images and corresponding size distribution of the resultant products (Figure 3) revealed that the average diameter of the Co NPs gradually increased from ca. 9 to ca. 27 nm with increasing pyrolysis temperature from 600 to 900 °C. This structural change was also reflected in the XRD patterns. As shown in Figure S3, all XRD patterns of the

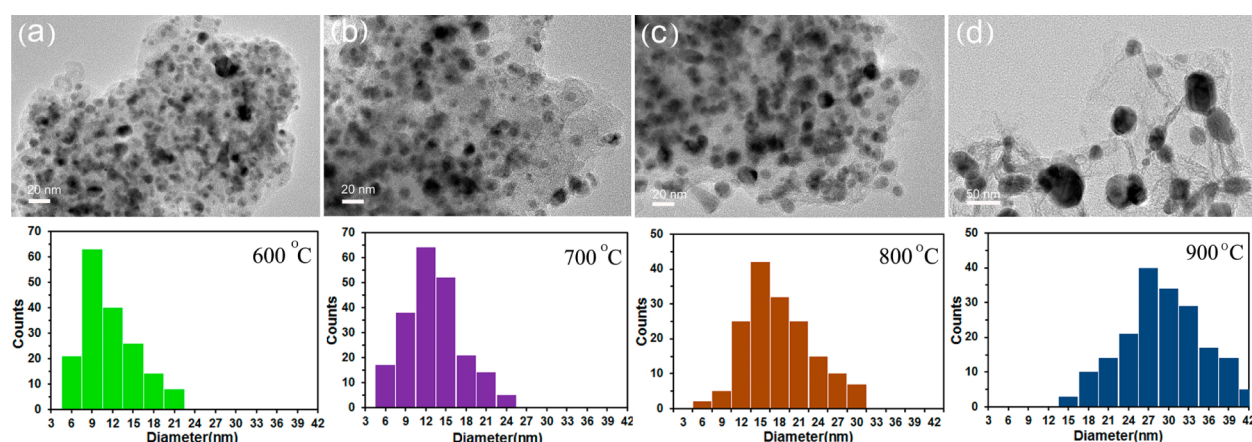


Figure 3. TEM images and corresponding size distribution of Co NPs synthesized by carbonizing the ZIF-67 precursor at different temperature: (a) 600 °C, (b) 700 °C, (c) 800 °C, and (d) 900 °C.

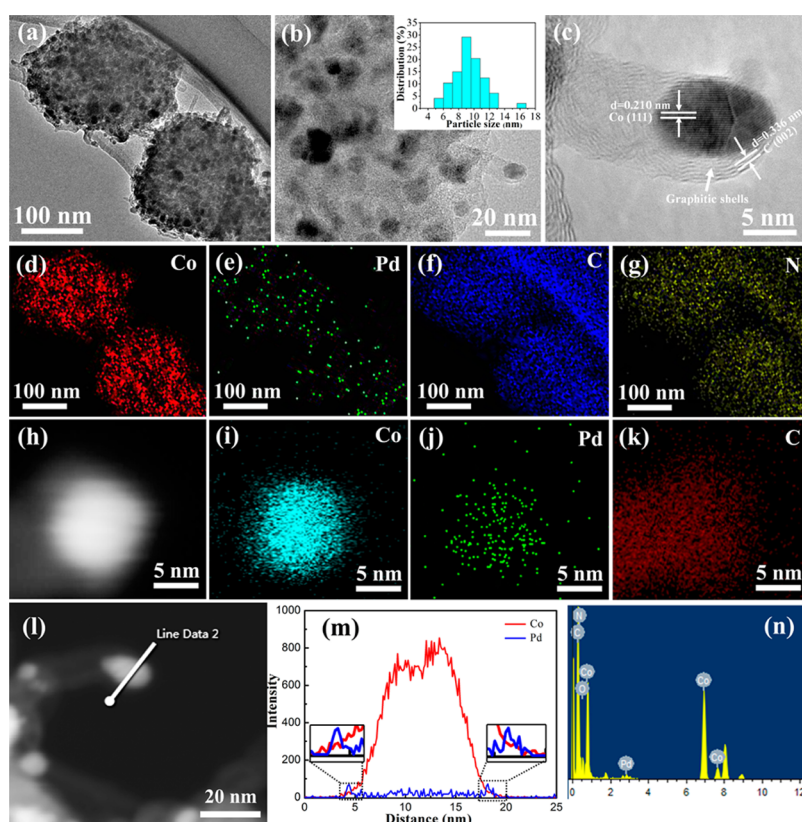


Figure 4. (a) and (b) TEM images of the Co@Pd/NC. The inset showed the corresponding size distribution of Co@Pd NPs. (c) HRTEM image of a Co@Pd nanoparticle. (d–g) Low-magnification EDX spectra of Co, Pd, C and N for a Co@Pd/NC particle. (h) HAADF-STEM image of an individual Co@Pd NPs and (i–k) the corresponding STEM-EDX elemental mapping images of Co and Pd. (m) Elemental line-scanning profiles along the direction marked by a white line in (l). (n) EDX spectrum of the Co@Pd/NC.

calcined composites showed three diffraction peaks at around 44.2, 51.6, and 76.0°, respectively, which were characteristic of metallic Co (JCPDS No. 15-0806).^{14,18} Note that the higher the calcination temperature, the narrower the peak width and the stronger the peak intensity. These suggested that the Co NPs in the products turned bigger in size and the crystallinity became better as the calcination temperature increased. According to the Scherrer equation (using the 44.2° (111) peak),¹⁹ the average size of the Co NPs obtained at 600 °C was estimated to be 8.1 nm, much smaller than that (24.6 nm) of the sample obtained at 900 °C, which were nearly matched

with the observed values from TEM. Raman spectroscopy had also been performed to determine the structural features of the carbonized samples (Figure S4). As expected, two predominant peaks at 1339 and 1581 cm⁻¹ were observed for all samples, corresponding to the D and G bands, respectively. The relative ratios of the D band to the G band illustrated the degree of graphitization.²⁰ The I_D/I_G of Co/NC (namely, the sample prepared by carbonizing ZIF-67 at 600 °C for 8 h) was around 1.57, which suggested the graphitic character of carbon species in Co/NC was not well developed, and the obtained carbon structures contain both graphene layers and disordered carbons.

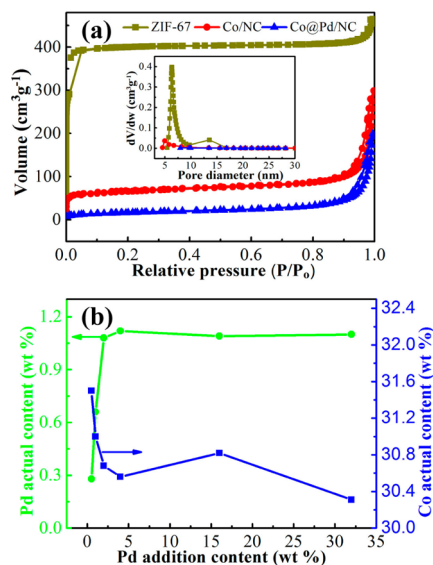


Figure 5. (a) Nitrogen adsorption/desorption isotherms at 77 K and Horvath–Kawazoe pore-size distribution curves (inset) of the ZIF-67, Co/NC, and Co@Pd/NC. (b) The Pd and Co actual content of the final products as a function Pd addition content.

Furthermore, increasing the carbonizing temperature and the duration of calcination both slightly increased the degree of graphitization of the obtained porous carbon. In addition, the low calcination temperature was obviously in favor of retaining nitrogen content of the final material (Table S1), which were widely regarded as an effective way to enhance the performance of carbon materials.²¹ Thus, we set the calcination temperature to be 600 °C and the resulting sample was denoted as Co/NC.

As observed from Figure 2b,c, both the Co/NC and Co@Pd/NC retained the similar size (~150 nm) and shape (concave cubes) as the ZIF-67 precursors. However, the

surface of the particles became fairly rougher than the ZIF-67 precursor, indicating the complete decomposition and carbonization of the zeolitic imidazolate framework. Compared to strong peaks that originated from ZIF-67 in XRD patterns (Figure 2d), characteristic peaks associated with metallic Pd within the Co@Pd/NC were too weak to be observed clearly, presumably because of their low concentrations and/or small sizes.²² However, their existence was confirmed by XPS (Figure 2e and S6) and AAS analyses (Table S2). In the Pd 3d XPS spectra of Co@Pd/NC illustrated in Figure 2e, two obvious peaks of Pd 3d_{5/2} and Pd 3d_{3/2} appeared at binding energies of 335.76 and 341.06 eV, respectively, which were close to, but lower by ~0.3 eV than that of monometallic Pd⁰ on activated charcoal (Pd/C, 336.06 and 341.36 eV). This implied that the Pd was existed in the metallic form in the Co@Pd/NC.²³ The peak shift of Pd⁰ to lower values might be attributable to the ultrafine size of Pd shell and the additional electron donating effect from inner Co atom to shell Pd atom.²⁴ Interestingly, the surface atomic ratio of Pd to Co was determined to be 0.21 from their peak areas after correction of sensitivity factors (Figure 2e, S6 and S7), which was much higher than the Pd/Co ratio determined in the bulk by AAS measurement (0.018) and TEM-EDX analysis (0.024) (Table S2 and Figure 4n), indicating that Co cores had been covered by Pd shell. The N 1s XPS spectra of Co/NC (Figure 2f) further shown the presence of two types of nitrogen species, which could be attributed to pyridinic (399.1 eV) and graphitic (401.0 eV) nitrogen atoms,²⁵ indicating that the N atoms were doped successfully into the Co/NC. However, the binding energy of pyridinic N shifted to higher value than those of metal-free N-doped graphene,²⁵ probably due to the electron redistribution after ionization and strong coordination interaction between Co and N atoms (Figure S8).²⁶ As expected, coverage of Co cores by Pd shells gently weakened the coordination interaction between Co and N atoms, as declared by the peak shift of pyridinic N for Co@Pd/NC to lower values compared with

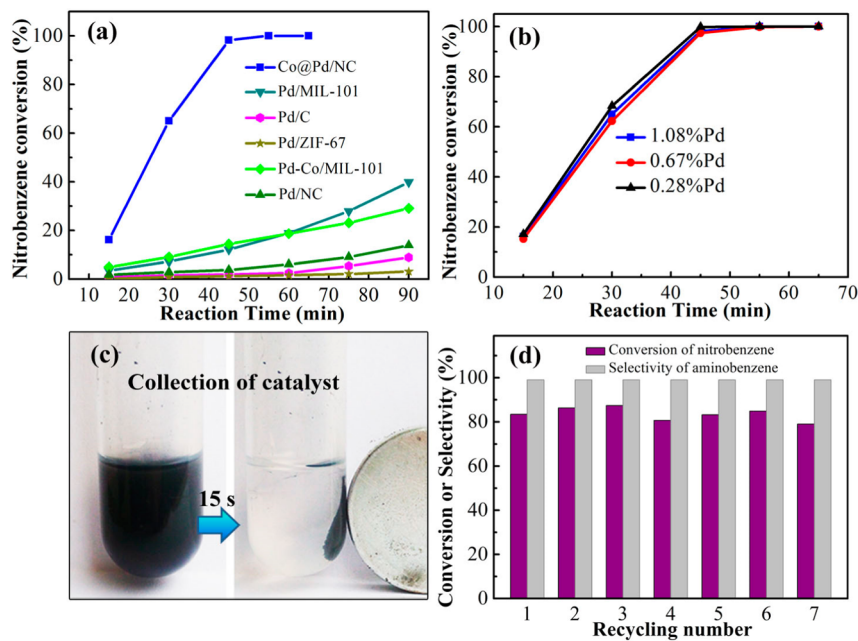
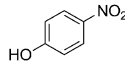
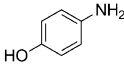
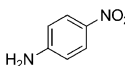
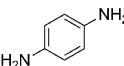
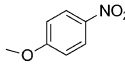
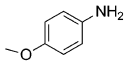
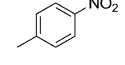
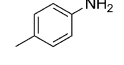
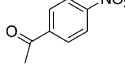
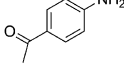
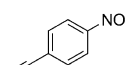
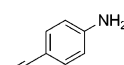
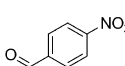
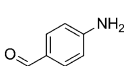
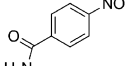
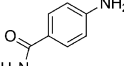
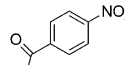
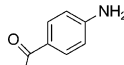
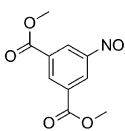
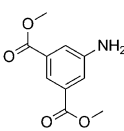
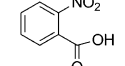
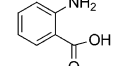
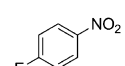
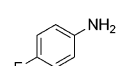
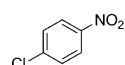
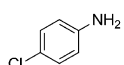
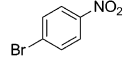
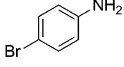


Figure 6. (a) Nitrobenzene conversions over various catalysts as a function of reaction time. (b) Effect of Pd content on the catalytic performance of the Co@Pd/NC-X (X was the Pd content). (c) Magnetic separation of the Co@Pd/NC. (d) Recyclability of the Co@Pd/NC in the hydrogenation of nitrobenzene.

Table 1. Hydrogenation of Various Substituted Nitroarenes over Co@Pd/NC Catalyst^a

| Entry | Substrate | Product | Time (min) | Conv. (%) | Sel. (%) |
|-------|---|---|------------|-----------|----------|
| 1 |  |  | 60 | >99 | >99 |
| 2 |  |  | 45 | 98 | >99 |
| 3 |  |  | 45 | >99 | >99 |
| 4 |  |  | 45 | >99 | >99 |
| 5 |  |  | 45 | >99 | >99 |
| 6 |  |  | 60 | >99 | >99 |
| 7 |  |  | 60 | 97 | 98 |
| 8 |  |  | 45 | 98 | >99 |
| 9 |  |  | 45 | 94 | >99 |
| 10 |  |  | 45 | 96 | >99 |
| 11 |  |  | 60 | >99 | >99 |
| 12 |  |  | 45 | 98 | >99 |
| 13 |  |  | 120 | >99 | >99 |
| 14 |  |  | 1320 | 93 | >99 |

^aReaction conditions: 0.5 mmol nitroarenes in 2 mL of EtOAc, magnetically stirring, H₂ balloon (1 atm), room temperature, catalysts: 0.2 mol % Pd.

Co/NC. The further quantitative analysis of the XPS results revealed that the N contents in Co/NC and Co@Pd/NC were as high as 7.9 and 7.4 wt %, respectively. These findings illustrated the absence of oxygen atoms in ZIF-67 precursor could retain effectively the nitrogen content in the final material.

More structural information for Co@Pd/NC was further revealed by TEM characterization. Ultrasonic treatment (30 min) of the sample for TEM tests was unable to break the Co@

Pd/NC particles, indicating their good mechanical stability (Figure 4a). As shown in Figure 4b, Co@Pd NPs were highly dispersed and embedded in a ligand-derived porous carbon matrix. The average size of Co@Pd NPs was determined to be 9.4 nm (Figure 4b), similar to that of starting Co nanoparticles, because shell layer formation and core metal consumption occurred simultaneously. Figure 4c highlighted the typical high-resolution TEM (HRTEM) image of a Co@Pd particle, which was embedded in layered graphitic carbon structures with a typical distance value of graphite (0.336 nm).²⁷ It was worth noting that only one type of crystal lattice was observed on the Co@Pd nanoparticle. These clearly resolved interplanar fringes were measured to be 0.223 nm, which should be ascribed to the crystal lattice of the (111) planes of face-centered cubic (fcc) Co.¹⁸ This meant the host Co matrix was well retained. The absence of Pd interplanar fringes should be due to the ultrafine size of Pd shell. Low-magnification EDX images (Figure 4d–4g) confirmed the homogeneous three-dimensional distribution of the Pd throughout the interior of the Co@Pd/NC particles and high-magnification EDX images (Figure 4h–4k) clearly revealed the coexistence of Co and Pd in an individual nanoparticle, which was surrounded by N-doped carbon. The presence of uniform Pd and Co in this nanoparticle was consistent with either CoPd alloys or the formation of the proposed Co@Pd core–shell particles. However, the EDX line scan (Figure 4m) taken along the line marked in Figure 4l showed a Co-rich core and an ultrathin Pd-rich shell, indicating the successful preparation of Co@Pd core–shell nanomaterial. From the EDX spectra in Figure 4n, Pd, Co, C, and N signals could be observed, reconfirming the existence of these four elements. The Pd/Co atomic ratio was determined to be 0.024, roughly consistent with the measured ratio of 0.018 by AAS measurement.

The polymerization and carbonization of imidazolate framework produced substantial meso/macropores, leading to a different pore structure from the ZIF-67 precursor. As shown in Figure 5a, the curves for ZIF-67 were a bit similar to the I-type isotherms,^{16,17,28} suggesting its dominating microporous characteristic. However, isotherms of the Co/NC exhibited a typical adsorption curve of type I plus IV with an apparent enhanced uptake and an obvious hysteresis loop in the P/Po range of 0.8–1,^{14,28} indicating its remarkable micro/meso-/macroporous structure (inset in Figure 5a and Figure S9). Interestingly, with the introduction of Pd in Co/NC, a huge drop in surface area was observed mainly from a decrease in micropore surface area (Table S2). As a result, the Co@Pd/NC showed a meso/macropore volume of 0.34 cm³/g, which was similar to that of Co/NC (0.37 m³/g) and 3.9-fold higher than that of the ZIF-67 precursor (0.09 m³/g). Because the larger pores remarkably facilitated physical transport,²⁹ the accessible meso-/macroporous structure of Co@Pd/NC could effectively enhance the mass and heat transfer of guest molecules and also the utilization of catalyst. In order to uncover the reason why the surface area dropped so significantly after Pd deposition, we conducted another comparative experiment where 0.4 g of as-prepared Co/NC was initially dispersed in 20 mL of acetone via ultrasonication and then agitated under magnetic stirring at room temperature for 12 h. After recovering, washing and drying, the BET surface area and pore size measurements were measured over the obtained solid (denoted as Co/NC-ace) by N₂ adsorption/desorption isotherms. As observed from Figure S10, the N₂ adsorption/desorption isotherms of the Co/NC-ace was very similar to that of Co@Pd/NC. Accordingly, the

BET surface area of Co/NC-ace also decreased from 239.7 to 59.7 m² g⁻¹. These results indicated the significant decrease of BET for Co@Pd/NC was caused by the destructive effect of acetone on the micropores rather than the Pd deposition, possibly due to capillary-force-driven channel collapse during removal of acetone solvent. It is well-known that galvanic replacement reaction has emerged as a powerful synthetic approach for converting solid metal nanostructures into hollow ones.³⁰ However, a control experiment with different Pd inventory indicated the galvanic replacement reaction could reach the thermodynamic equilibrium in our work with a maximal Pd loading of ca. 1.1 wt % (Figure 5b), indicating the surface coating with N-doped carbon shells could effectively facilitate the formation of ultrathin Pd shell and thus minimize the use of Pd. In addition, with increasing the Pd dosage from 0.5 to 2 wt %, the Pd actual content of the final product increased from 0.3 to 1.1 wt % and the Co actual content decreased from 31.5 to 30.3 wt %, signifying the gradual galvanic replacement of Co by Pd.

The catalytic activities of the Co@Pd/NC were tested and compared with the pristine ZIF-67 supporting Pd NPs (Pd/ZIF-67, Figure S11), the most-used MIL-101 supporting Pd NPs (Pd/MIL-101, Figure S12), and Pd-Co NPs (Pd-Co/MIL-101, Figure S13), the activated charcoal supporting Pd NPs (Pd/C, Figure S14), and the Co-free NC supporting Pd NPs (Pd/NC, Figure S15), using the hydrogenation of nitrobenzene as a model reaction. Reactions were performed at room temperature and atmospheric pressure of H₂ under base-free conditions. As shown in Figure 6a, the Pd/C and Pd/ZIF-67 were almost inactive for this reaction. After 90 min of reaction, the conversion of nitrobenzene over Pd/C and Pd/ZIF-67 were only 9% and 3%, respectively. The Pd/MIL-101 as a conventional hydrogenation catalyst showed moderate activity, giving 40% conversion of nitrobenzene after 90 min of reaction. In sharp contrast, the Co@Pd/NC exhibited extremely high activity with a 98% conversion of nitrobenzene within only 45 min of reaction. In fact, our Co@Pd/NC catalyst was also the most active for hydrogenation of nitrobenzene among a number of supported Pd catalysts (Table S3). The high activity of Co@Pd/NC must have been originated from the highly exposed Pd atom on Co cores,³¹ as our preliminary test showed that the Co/NC itself was essentially inactive for this reaction under the investigated conditions. The role of N in the Co@Pd/NC's activity was evaluated by a referential catalyst prepared by first etching away the Co NPs in Co/NC and then loading Pd NPs over the obtained N-doped porous carbon (namely, Pd/NC). Interesting, the Pd/NC showed slightly higher hydrogenation activity than the Pd/C, indicating the synergistic effect of the N with Pd NPs also enhanced the catalytic activity. In addition, the Pd-Co/MIL-101 showed a bit lower activity than Pd/MIL-101, as indicated by the relatively lower conversion (~29%) after 90 min of reaction, maybe due to its large particle size, indicating the synergistic effect of Pd with Co was not important to the enhanced activity. Further, it was worth noting that the Co@Pd/NC-X with different Pd contents showed similar catalytic activities for this reaction, indicating their excellent efficiency and applicability (Figure 6b and Table S3).

The recyclability of the Co@Pd/NC was further investigated under an appropriate reaction condition (0.67 mmol nitrobenzene in 2 mL EtOAc, magnetically stirring, H₂ balloon, room temperature, catalysts: 0.15 mol % Pd, 45 min of reaction time). After the reaction, the Co@Pd/NC was easily separated

from the reaction solution by the magnet (Figure 6c), implying its good magnetic properties. As shown in Figure 6d, the Co@Pd/NC could be regenerated and reused at least seven times in the subsequent reaction without significant decreases in catalytic activity and selectivity. In addition, after removing the solids from the reaction mixture after 15 min of reaction time and stirring the reaction solution for additional 30 min, no further conversion of nitrobenzene was observed, which confirmed that the reaction catalyzed by Co@Pd/NC was truly heterogeneous. This finding was in good agreement with AAS experiments where no Pd traces were detected in the reaction solution. Further investigation of the substrate scope was performed under the same reaction conditions. As summarized in Table 1, our Co@Pd/NC showed good tolerance to a broad scope of substituted nitroarenes containing -OH, -CHO, -CN, -CO, -COOC, -CON, and -X functional groups. For all substrates, the selectivity to functionalized anilines was ≥98% at the nitroarene conversion level of ≥93%. Besides, the slowly dissolving nitroarenes containing Br or Cl groups (Table 1, entries 13 and 14) needed much more time to complete than the F-substituent nitroarene, which has a high solubility in EtOAc (entry 12).

CONCLUSION

We have developed an MOFs-templated strategy to prepare Co@Pd core-shell nanoparticles by using MOFs-derived Co NPs as sacrificial template to reduce an aqueous Pd(NO₃)₂ via galvanic replacement reaction. The small Pd@Co shell-core nanoparticles embedded in the N-doped carbon matrix were highly dispersed with an average size of ca. 9 nm and a maximum Pd loading of ca. 1.1 wt %. XPS analysis, AAS measurement and line-scanning profiling analysis together confirmed the successful coverage of MOFs-derived Co NPs by ultrathin Pd shell. Particularly, when being used in hydrogenation of nitrobenzene, our Co@Pd/NC showed much higher hydrogenation activity than MOFs supporting noble NPs. The present work might open a new avenue for artificially designed MOFs-templated non-noble@noble metal core-shell nanocatalysts that could far surpass the traditional MOFs supporting noble NPs in catalytic properties.

ASSOCIATED CONTENT

Supporting Information

The Supporting Information is available free of charge on the ACS Publications website at DOI: 10.1021/acscatal.5b00998.

Additional SEM and TEM images, XRD patterns, BJH pore size distributions, TG curves, XPS spectrum, and other supplemental data (PDF)

AUTHOR INFORMATION

Corresponding Author

*E-mail: liyw@scut.edu.cn.

Notes

The authors declare no competing financial interest.

ACKNOWLEDGMENTS

We thank the National Natural Science Foundation of China (21322606 and 21436005), the Doctoral Fund of Ministry of Education of China (20120172110012), China Postdoctoral Science Foundation (2015M572323), Fundamental Research Funds for the Central Universities (2015ZM045, 2015ZP002, and 2015PT004) and Guangdong Natural Science Foundation

(2014A030310445, 2013B090500027, and 10351064101000000) for financial support.

REFERENCES

- (1) (a) Cui, Y.; Yue, Y.; Qian, G.; Chen, B. *Chem. Rev.* **2011**, *112*, 1126–1162. (b) Latroche, M.; Surblé, S.; Serre, C.; Mellot-Draznieks, C.; Llewellyn, P. L.; Lee, J. H.; Chang, J. S.; Jhung, S. H.; Férey, G. *Angew. Chem., Int. Ed.* **2006**, *45*, 8227–8231. (c) Hwang, Y. K.; Hong, D. Y.; Chang, J. S.; Jhung, S. H.; Seo, Y. K.; Kim, J.; Vimont, A.; Daturi, M.; Serre, C.; Férey, G. *Angew. Chem., Int. Ed.* **2008**, *47*, 4144–4148. (d) Cavka, J. H.; Jakobsen, S.; Olsbye, U.; Guillou, N.; Lamberti, C.; Bordiga, S.; Lillerud, K. P. *J. Am. Chem. Soc.* **2008**, *130*, 13850–13851. (e) Li, H.; Eddaoudi, M.; O’Keeffe, M.; Yaghi, O. M. *Nature* **1999**, *402*, 276–279. (f) Férey, G.; Mellot-Draznieks, C.; Serre, C.; Millange, F.; Dutour, J.; Surblé, S.; Margiolaki, I. *Science* **2005**, *309*, 2040–2042.
- (2) (a) Lee, J.; Farha, O. K.; Roberts, J.; Scheidt, K. A.; Nguyen, S. T.; Hupp, J. T. *Chem. Soc. Rev.* **2009**, *38*, 1450–1459. (b) Corma, A.; Garcia, H.; Llabrés i Xamena, F. *Chem. Rev.* **2010**, *110*, 4606–4655. (c) Farrusseng, D.; Aguado, S.; Pinel, C. *Angew. Chem., Int. Ed.* **2009**, *48*, 7502–7513. (d) Liu, J.; Chen, L.; Cui, H.; Zhang, J.; Zhang, L.; Su, C.-Y. *Chem. Soc. Rev.* **2014**, *43*, 6011–6061.
- (3) (a) Hermes, S.; Schröter, M. K.; Schmid, R.; Khodeir, L.; Muhler, M.; Tissler, A.; Fischer, R. W.; Fischer, R. A. *Angew. Chem., Int. Ed.* **2005**, *44*, 6237–6241. (b) Hermes, S.; Schröter, F.; Amirjalayer, S.; Schmid, R.; Fischer, R. A. *J. Mater. Chem.* **2006**, *16*, 2464–2472.
- (4) (a) Yuan, B.; Pan, Y.; Li, Y.; Yin, B.; Jiang, H. *Angew. Chem., Int. Ed.* **2010**, *49*, 4054–4058. (b) Pan, Y.; Ma, D.; Liu, H.; Wu, H.; He, D.; Li, Y. *J. Mater. Chem.* **2012**, *22*, 10834–10839. (c) Sabo, M.; Henschel, A.; Fröde, H.; Klemm, E.; Kaskel, S. *J. Mater. Chem.* **2007**, *17*, 3827–3832.
- (5) (a) Jiang, H.-L.; Liu, B.; Akita, T.; Haruta, M.; Sakurai, H.; Xu, Q. *J. Am. Chem. Soc.* **2009**, *131*, 11302–11303. (b) Ishida, T.; Nagaoka, M.; Akita, T.; Haruta, M. *Chem. - Eur. J.* **2008**, *14*, 8456–8460.
- (6) (a) Liu, H.; Li, Y.; Jiang, H.; Vargas, C.; Luque, R. *Chem. Commun.* **2012**, *48*, 8431–8433. (b) Liu, H.; Liu, Y.; Li, Y.; Tang, Z.; Jiang, H. *J. Phys. Chem. C* **2010**, *114*, 13362–13369.
- (7) (a) Aijaz, A.; Karkamkar, A.; Choi, Y. J.; Tsumori, N.; Rönnebro, E.; Autrey, T.; Shioyama, H.; Xu, Q. *J. Am. Chem. Soc.* **2012**, *134*, 13926–13929. (b) Zhu, Q.-L.; Li, J.; Xu, Q. *J. Am. Chem. Soc.* **2013**, *135*, 10210–10213. (c) Yadav, M.; Xu, Q. *Chem. Commun.* **2013**, *49*, 3327–3329. (d) Chen, Y.-Z.; Zhou, Y.-X.; Wang, H.; Lu, J.; Uchida, T.; Xu, Q.; Yu, S.-H.; Jiang, H.-L. *ACS Catal.* **2015**, *5*, 2062–2069.
- (8) (a) Mustafa, D.; Breynaert, E.; Bajpe, S. R.; Martens, J. A.; Kirschhock, C. E. *Chem. Commun.* **2011**, *47*, 8037–8039. (b) Sun, J.-K.; Xu, Q. *Energy Environ. Sci.* **2014**, *7*, 2071–2100.
- (9) (a) Zhang, W.; Hu, Y.; Ge, J.; Jiang, H.-L.; Yu, S.-H. *J. Am. Chem. Soc.* **2014**, *136*, 16978–16981. (b) Yang, S. J.; Park, C. R. *Adv. Mater.* **2012**, *24*, 4010–4013.
- (10) (a) Decoste, J. B.; Peterson, G. W.; Smith, M. W.; Stone, C. A.; Willis, C. R. *J. Am. Chem. Soc.* **2012**, *134*, 1486–1489. (b) DeCoste, J. B.; Peterson, G. W.; Schindler, B. J.; Killops, K. L.; Browe, M. A.; Mahle, J. J. *J. Mater. Chem. A* **2013**, *1*, 11922–11932.
- (11) (a) DeCoste, J. B.; Peterson, G. W.; Jasuja, H.; Glover, T. G.; Huang, Y.-g.; Walton, K. S. *J. Mater. Chem. A* **2013**, *1*, S642–S650. (b) Liu, T.-F.; Zou, L.; Feng, D.; Chen, Y.-P.; Fordham, S.; Wang, X.; Liu, Y.; Zhou, H.-C. *J. Am. Chem. Soc.* **2014**, *136*, 7813–7816.
- (12) (a) Talin, A. A.; Centrone, A.; Ford, A. C.; Foster, M. E.; Stavila, V.; Haney, P.; Kinney, R. A.; Szalai, V.; El Gabaly, F.; Yoon, H. P.; et al. *Science* **2014**, *343*, 66–69. (b) Yin, Z.; Wang, Q.-X.; Zeng, M.-H. *J. Am. Chem. Soc.* **2012**, *134*, 4857–4863.
- (13) (a) Kim, T. K.; Lee, K. J.; Cheon, J. Y.; Lee, J. H.; Joo, S. H.; Moon, H. R. *J. Am. Chem. Soc.* **2013**, *135*, 8940–8946. (b) Zhang, Y.-F.; Qiu, L.-G.; Yuan, Y.-P.; Zhu, Y.-J.; Jiang, X.; Xiao, J.-D. *Appl. Catal., B* **2014**, *144*, 863–869. (c) Amali, A. J.; Hoshino, H.; Wu, C.; Ando, M.; Xu, Q. *Chem. - Eur. J.* **2014**, *20*, 8279–8282.
- (14) (a) Das, R.; Pachfule, P.; Banerjee, R.; Poddar, P. *Nanoscale* **2012**, *4*, 591–599. (b) Zhong, W.; Liu, H.; Bai, C.; Liao, S.; Li, Y. *ACS Catal.* **2015**, *5*, 1850–1856.
- (15) Qian, J.; Sun, F.; Qin, L. *Mater. Lett.* **2012**, *82*, 220–223.
- (16) Banerjee, R.; Phan, A.; Wang, B.; Knobler, C.; Furukawa, H.; O’Keeffe, M.; Yaghi, O. M. *Science* **2008**, *319*, 939–943.
- (17) Shi, Q.; Chen, Z.; Song, Z.; Li, J.; Dong, J. *Angew. Chem., Int. Ed.* **2011**, *50*, 672–675.
- (18) Nam, K. M.; Shim, J. H.; Ki, H.; Choi, S. I.; Lee, G.; Jang, J. K.; Jo, Y.; Jung, M. H.; Song, H.; Park, J. T. *Angew. Chem., Int. Ed.* **2008**, *47*, 9504–9508.
- (19) Zhang, F.; Yuan, C.; Zhu, J.; Wang, J.; Zhang, X.; Lou, X. W. D. *Adv. Funct. Mater.* **2013**, *23*, 3909–3915.
- (20) Wu, Z. S.; Winter, A.; Chen, L.; Sun, Y.; Turchanin, A.; Feng, X.; Müllen, K. *Adv. Mater.* **2012**, *24*, 5130–5135.
- (21) (a) Zheng, X.; Deng, J.; Wang, N.; Deng, D.; Zhang, W. H.; Bao, X.; Li, C. *Angew. Chem., Int. Ed.* **2014**, *53*, 7023–7027. (b) Xu, X.; Tang, M.; Li, M.; Li, H.; Wang, Y. *ACS Catal.* **2014**, *4*, 3132–3135. (c) Gao, Y.; Hu, G.; Zhong, J.; Shi, Z.; Zhu, Y.; Su, D. S.; Wang, J.; Bao, X.; Ma, D. *Angew. Chem., Int. Ed.* **2013**, *52*, 2109–2113.
- (22) Li, X.; Guo, Z.; Xiao, C.; Goh, T. W.; Tesfagaber, D.; Huang, W. *ACS Catal.* **2014**, *4*, 3490–3497.
- (23) (a) McEleney, K.; Crudden, C. M.; Horton, J. H. *J. Phys. Chem. C* **2009**, *113*, 1901–1907. (b) Yamada, Y. M. A.; Yuyama, Y.; Sato, T.; Fujikawa, S.; Uozumi, Y. *Angew. Chem., Int. Ed.* **2014**, *53*, 127–131.
- (24) Long, J.; Liu, H.; Wu, S.; Liao, S.; Li, Y. *ACS Catal.* **2013**, *3*, 647–654.
- (25) (a) Chen, L.; Xu, C.; Du, R.; Mao, Y.; Xue, C.; Chen, L.; Qu, L.; Zhang, J.; Yi, T. *J. Mater. Chem. A* **2015**, *3*, 5617–5627. (b) Xue, Y.; Liu, J.; Chen, H.; Wang, R.; Li, D.; Qu, J.; Dai, L. *Angew. Chem., Int. Ed.* **2012**, *51*, 12124–12127.
- (26) Wang, H.; Maiyalagan, T.; Wang, X. *ACS Catal.* **2012**, *2*, 781–794.
- (27) Tang, J.; Salunkhe, R. R.; Liu, J.; Torad, N. L.; Imura, M.; Furukawa, S.; Yamauchi, Y. *J. Am. Chem. Soc.* **2015**, *137*, 1572–1580.
- (28) Khalfaoui, M.; Knani, S.; Hachicha, M.; Lamine, A. B. *J. Colloid Interface Sci.* **2003**, *263*, 350–356.
- (29) (a) Groen, J. C.; Zhu, W.; Brouwer, S.; Huynink, S. J.; Kapteijn, F.; Moulijn, J. A.; Pérez-Ramírez, J. *J. Am. Chem. Soc.* **2007**, *129*, 355–360. (b) Shen, K.; Qian, W.; Wang, N.; Zhang, J.; Wei, F. *J. Mater. Chem. A* **2013**, *1*, 3272–3275. (c) Shen, K.; Wang, N.; Qian, W.; Cui, Y.; Wei, F. *Catal. Sci. Technol.* **2014**, *4*, 3840–3844. (d) Shen, K.; Qian, W.; Wang, N.; Su, C.; Wei, F. *J. Mater. Chem. A* **2014**, *2*, 19797–19808. (e) Shen, K.; Qian, W.; Wang, N.; Su, C.; Wei, F. *J. Am. Chem. Soc.* **2013**, *135*, 15322–15325.
- (30) (a) Liang, H. P.; Zhang, H. M.; Hu, J. S.; Guo, Y. G.; Wan, L. J.; Bai, C. L. *Angew. Chem., Int. Ed.* **2004**, *43*, 1540–1543. (b) Zhang, W.; Yang, J.; Lu, X. *ACS Nano* **2012**, *6*, 7397–7405.
- (31) (a) Zhang, N.; Liu, S.; Xu, Y.-J. *Nanoscale* **2012**, *4*, 2227–2238. (b) Zhang, N.; Xu, Y.-J. *Chem. Mater.* **2013**, *25*, 1979–1988. (c) Liu, S.; Zhang, N.; Xu, Y. J. *Part. Part. Syst. Charact.* **2014**, *31*, 540–556.